Stall Transients of Axial Compression Systems with Inlet Distortion

F. K. Moore*
Cornell University, Ithaca, New York

A previously derived system of differential equations, based on fluid mechanics, is extended to provide a theory to predict how rotating stall or surge will develop in an axial compression system under combined influences of inlet distortion and throttle ramping. Results are relevant to the problem of stagnation stall of gas turbines. It is found that stall margin is improved by large aerodynamic lag in the compressor. Both stall and recovery transients are considered. A distinction between axisymmetric and in-rotating-stall compressor performance characteristics leads to a concept of rotating-stall stability that explains the appearance of classic stall at low stage loading and the hysteresis associated with rotating stall. The influences of various system parameters are systematically explored, and the large *B* parameter, tall compressor characteristic diagram, and rapid throttle closure are all found to favor surge, while large distortion and small shut-off head relative to peak pressure rise both favor rotating stall. When surge occurs, rotating stall is usually also present.

Nomenclature†

A = amplitude of angular disturbance
a = reciprocal time lag, chiefly inertial, of the compressor[1,5]
A_c = compressor duct area
a_s = sound speed
g = disturbance of axial flow coefficient
h = circumferential velocity coefficient
J = square of amplitude of angular disturbance A
K = parameter, $3\ell_c/(m+1/a)$
K_T = throttle coefficient
ℓ_B = blade-passage length (blade chord)
ℓ_c = total flow length from entrance to plenum
ℓ_d = flow length equal to $\ell_c-(m+1/a)$
m = coefficient depending on entrance and exit duct flows[1,5]
N = number of stages
P = expression for angle-averaged pressure coefficient
p_S = static pressure at end of exit duct in plenum
p_T = total pressure of supply and return reservoirs
Q = expression for angle-averaged axial flow coefficient
r = phase angle between distortion and compressor disturbance
T = modified dimensionless time (see also ξ) equal to $\xi\,(H/W)/\ell_c$
U = wheel speed at mean diameter
V_p = volume of plenum
y = axial distance downstream from compressor face
γ = blade stagger angle
ϵ = amplitude of velocity distortion
θ = angular coordinate, circumferentially around wheel
ξ = dimensionless time, relative to time for wheel to rotate one radian
Φ = annulus-averaged axial flow coefficient, relative to U
ϕ = local axial flow coefficient, a function of time and angle
Ψ = instantaneous total-to-static pressure-rise coefficient, relative to density times U^2
ψ_c = axisymmetric, steady pressure-rise characteristics
ψ_{c_0} = shut-off level of axisymmetric characteristic

Subscripts

0 = evaluated at the compressor face
∞ = evaluated far upstream, in the distorted shear flow
F = at a final throttle position
T = evaluated at the throttle

I. Introduction

A THEORY of stall transients of axial compression systems has been presented in Refs. 1 and 2 and, in somewhat more detail, in Ref. 3. That theory represents a combining of previous analyses of pure surge[4] and pure rotating stall.[5] The new theory consists of a set of differential equations able to represent pure surge or rotating stall as special cases and, more importantly, general transients of system operation which may evolve into surge or rotating stall. With suitable refinements and extensions, this theory should make it possible to relate the occurrence of "stagnation stall" to features of a compression system and to the nature of an imposed transient of its operation. The present paper represents such an extension.

References 1 and 2 showed the important influence of triggering mechanisms on the subsequent development of transients. To induce surge-like behavior, any time-dependent initial disturbance, for example, a slight throttle-valve change, will suffice. To induce rotating-stall-like behavior, some angular nonuniformity must be present; furthermore, Ref. 2 indicates that the strength of the nonuniformity can have a considerable effect on the evolution of a transient. An important source of angular nonuniformity is inlet total-head distortion, which is known to have an important effect on the stall margin of compression systems.[6]

Accordingly, this article extends the theory of Refs. 1 and 2 to include the simultaneous effects of valve movement and inlet distortion on the transient stall behavior of axial compression systems which are specified by given descriptive parameters. The interrelationships of the system parameters and the triggering disturbances are explored, to show the various types of transient motions that arise from solutions of the equations, and to explain and interpret these occurrences. Quantitative comparisons with test experience are not made here. However, results will be seen to be consistent with experience and will lead to inferences about design which may find important practical application in the future.

Received Aug. 8, 1985; revision received June 20, 1986.

*Professor, Mechanical and Aerospace Enginering, Sibley School of Mechanical and Aerospace Engineering. Fellow AIAA.

†Notation follows Ref. 1. Other notation is defined in Table 2. All lengths are relative to wheel radius.

II. Background of Analysis

Before the feature of inlet distortion is introduced, the analytical background provided by Ref. 1 should be summarized. Figure 1 sketches the idealized compression system consisting of an entrance duct, an axial compressor of N stages of annulus area A_c, an exit duct, a plenum of volume V_p, and a throttle duct and throttle of coefficient K_T which may be variable with time (in the forms ξ or T, as defined in the Nomenclature). The dimensionless flow-path length from entrance to plenum, including a tortuous section through the compressor, is ℓ_c. The quantities A_c and V_p are both subsumed in the familiar parameter B.[4] The wheel speed U is constant. Angle θ is measured around the wheel, and the dimensionless axial distance is y.

In Fig. 1 and in the present analysis, the entrance duct is assumed to have constant area, and the throttle duct is assumed to be very short. The flow is considered to be incompressible; therefore, the angle-averaged axial velocity coefficient Φ is constant through the entrance and compressor, though it may vary with time. The corresponding throttle flow coefficient Φ_T may also vary with time and differ in value from Φ. Flow enters the system from a reservoir at constant total pressure p_T. In the plenum, a pressure p_S is reached which may vary with time but not, of course, with angle. The throttle flow, also independent of angle, leads back to the reservoir pressure p_T.

An inviscid flow is assumed in the entrance duct. In this flow, the axial flow coefficient at the compressor face may undergo in angular variation denoted by g. This function will describe rotating stall should it occur. If g should be zero, the entrance flow will be straight and uniform. However, if the entrance flow should have a nonzero g, laws of fluid mechanics will provide that a transverse velocity component will appear, indicated by the function h at the compressor face. The angular variation of flow coefficient at the entrance of amplitude ϵ will describe the inlet distortion to be discussed later.

The parameter m[1,5] expresses the degree to which axial fluctuations g produce transverse fluctuations h in both the entrance and exit duct flowfields. In the configuration shown in Fig. 1, in which both entrance and exit ducts are long and straight, m is about 2. If the entrance is convergent or the exit duct is very short, m would be smaller. The parameter a (discussed in Refs. 1 and 5) is a coefficient of purely unsteady blade-passage pressure rise in the compressor resulting from axial acceleration. That is, any unsteadiness of ϕ is assumed to contribute a term $-(1/a)\partial\phi/\partial\xi$ to the pressure-rise coefficient ψ. In effect, a is a reciprocal time lag; it is inversely proportional to the number of stages.

The foregoing system (without inlet distortion) was analyzed in Refs. 1-3. An essential ingredient of that theory, and of the preceding Refs. 4 and 5, is the assumption that the "axisymmetric characteristic" of the compressor is known; that is, the coefficient ψ_c of total-to-static pressure rise $(p_S - p_T)$ which would apply in the absence of any time or angle variations. Furthermore, that function was taken to be a simple cubic as shown in Fig. 2 for reasons discussed there and in Ref. 7.

The rotating stall theory of Ref. 5 gives a steady performance result, or actual steady pressure rise coefficient Ψ, which is very different from the underlying axisymmetric characteristic ψ_c. Calculations in Refs. 7 and 9 give the result labeled "exact" on Fig. 2. An approximate solution of the rotating-stall equations, based on assuming a harmonic wave form and satisfying averages of the governing equation, was found in Ref. 1 and is shown as the "Galerkin" curve of Fig. 2. The corresponding Galerkin result for rotating-stall amplitude is shown as the dashed line A. These results are discussed in Ref. 1; here, rotating stall is only noted as a possibility when the flow coefficient lies in the zone where ψ_c has positive slope.

The axisymmetric characteristic has the features of height H, width W, and shut-off value ψ_{c0}. These features are additional system parameters to be specified. The quantity H is obviously proportional to loading per stage and number of stages. W depends inversely on blade stagger, and it may then immediately be shown that the steepness of the diagram H/W is proportional to both N and blade turning. Shut-off head is generally well represented as $0.11\,\rho U^2 N$ according to Ref. 8. Henceforth, ψ_{c_0} will appear in its ratio to H; that quantity PHO will thus be inversely proportional to stage loading. All pressure coefficients Ψ will be expressed as ratios to H, and flow coefficients Φ as ratios to W. In terms of the resulting quantities, called P and Q, the axisymmetric characteristic assumes a universal shape as shown in Fig. 3. Also, in Fig. 3 the Galerkin performance result for pure rotating stall is repeated.

The present analysis will assume that the throttle pressure drop is always proportional to Φ^2. Therefore, different throttle settings will appear as different parabolas in Fig. 3. A particular value of K_T in Fig. 1 would correspond to each of those

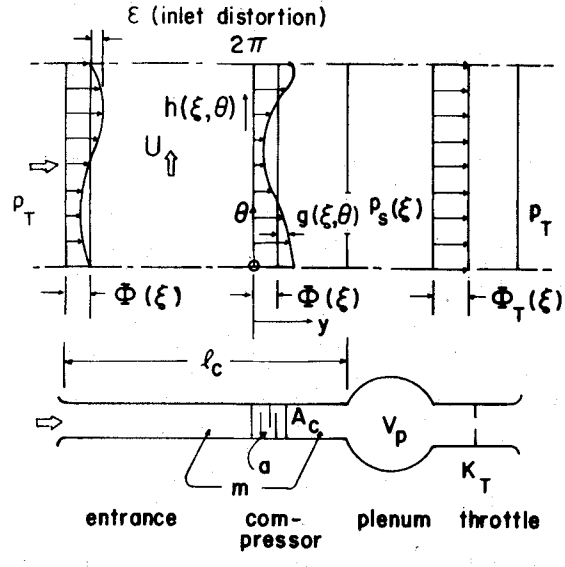

Fig. 1 Sketch of compression system and notation. Top view shows the axial flow coefficients at three locations as functions of angle θ.

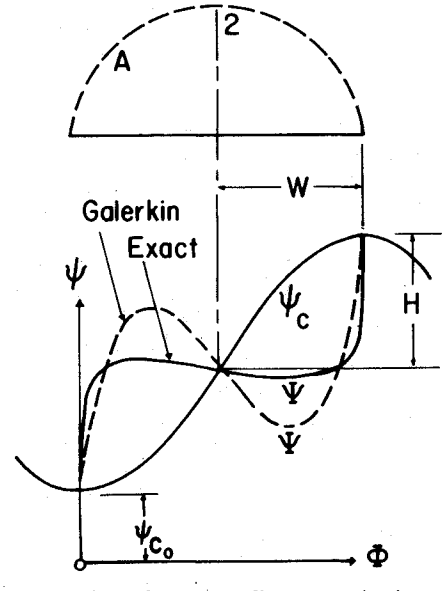

Fig. 2 Sketch of performance diagrams. ψ_c is axisymmetric characteristic, assumed cubic with features H, W, and ψ_{c_0}; actual performance in pure rotating stall is shown as Ψ (Galerkin or "Exact"). The Galerkin amplitude is A.

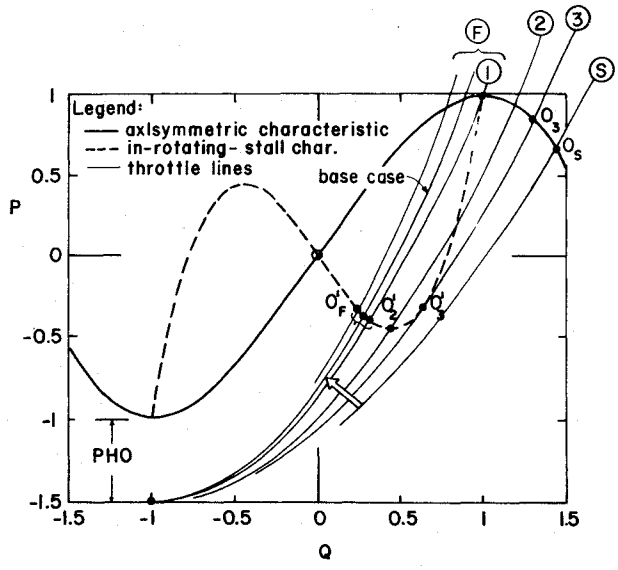

Fig. 3 Pressure-rise coefficient in form P vs Q for $PHO=0.5$; axisymmetric and in-rotating-stall characteristics and various possible throttle lines. Possible unstalled operating points are labeled O; corresponding points in pure rotating stall are labeled O'.

parabolas. For future use, certain special cases may be singled out. A stall episode might begin with the throttle at (S), for which only the unstalled operation point O_S is possible. If the throttle is closed to (3), two steady possibilities exist, namely points O_3 unstalled and O_3' in rotating stall. Line (2) is the one which happens to pass through the minimum of the rotating-stall characteristic. Line (1) passes through the maximum of the axisymmetric characteristic, and instability is expected to appear for more closed throttle lines, such as those labeled (F). Line (2) will be found to have a somewhat analogous significance for rotating stall.

In Sec. V, the stall resulting from dynamic throttle closure from position (S) to a final setting (F) is examined, and in Sec. VI, recovery from stall is examined by first closing the throttle to a deep stall condition and then opening it again. In advance, one may expect that results will depend on the "ramp rates" of throttle change during these processes.

In summary, we intend to study the simultaneous effects of inlet distortion and dynamic valve change on an ideal compression system characterized by the following dimensionless parameters: B, a, ℓ_c, m, H, W, and PHO. First, it is necessary to modify the governing equations of Ref. 1, in order to include inlet distortion.

III. Governing Equations with Inlet Distortion

Equations (59-61) of Ref. 1 will govern transients of the system shown in Fig. 1 without inlet distortion, subject to certain approximations in addition to those already mentioned. These additional approximations were fully discussed in Ref. 1, and they may be briefly summarized as follows: 1) An idealized relation was assumed to connect the disturbance velocities g and h; this simplifying relation seems to be quite accurate in general. 2) Any transverse velocity disturbance h will imply a misalignment of the flow with the entrance to the first row, presumably inlet guide vane (IGV); a head loss could occur because of the sudden turning required there. That IGV entrance loss was neglected. 3) A Galerkin method was used to average over angle. Thus, the equations were reduced to ordinary differential equations in time, and the angular variation of flow coefficient (as in rotating stall) was described by an amplitude function of time A.

In the original problem, radial and axial distances would have also been independent variables; however, radial variations were neglected, and axial variations were taken into account by flowfield theory in the ducts, and by the assumption

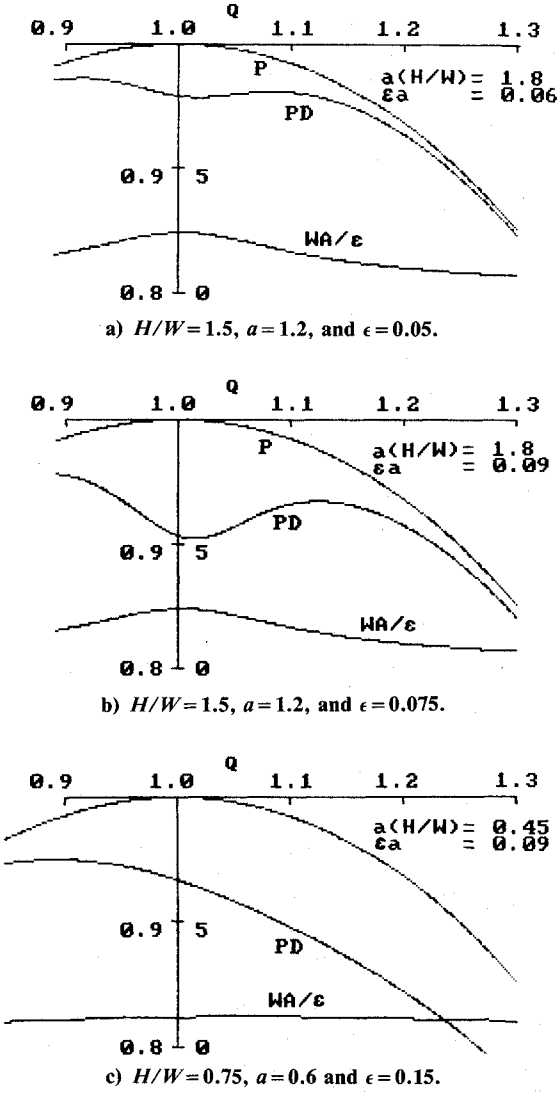

a) $H/W=1.5$, $a=1.2$, and $\epsilon=0.05$.

b) $H/W=1.5$, $a=1.2$, and $\epsilon=0.075$.

c) $H/W=0.75$, $a=0.6$ and $\epsilon=0.15$.

Fig. 4 Steady effects of distortion. ϵa governs loss of peak pressure rise; $a(H/W)$ governs value of flow coefficient at the peak.

of incompressible flow in repeating stages in the compressor. 4) The axisymmetric characteristic was taken to be cubic, as already discussed in reference to Figs. 2 and 3.

The foregoing assumptions will be maintained, but the resulting ordinary differential equations will now be modified to include the effects of harmonic inlet distortion. Figure 1 sketches a flow coefficient at the inlet given by

$$\phi_\infty = \Phi(\xi) - \epsilon \sin\theta \tag{1}$$

A parallel shear flow with constant static pressure and a constant velocity-distortion amplitude ϵ is assumed. In such a case, total pressure will not be constant. In principle, the inlet flowfield should be analyzed to account for the actual loss mechanisms which produce the distortion. The present distortion model is correct in the limit of a long entrance duct, so that the parallel shear flow becomes well established before any upstream effects of compressor disturbance g are felt.

For incompressible flow, Eq. (1) yields the following relation between the total-to-static pressure-rise coefficient Ψ and its angle-averaged value $\bar{\Psi}$

$$\Psi = \bar{\Psi} + \epsilon\Phi \sin\theta + \tfrac{1}{4}\epsilon^2 \cos 2\theta \tag{2}$$

In this study, it is $\bar{\Psi}$ which will be followed in a transient. A realistic entrance-flow study might modify the analysis at this point. For convenience, Φ and $\bar{\Psi}$ are replaced by the following

quantities

$$P \equiv (\bar{\Psi}/H) - 1 - PHO, \qquad Q \equiv (\Phi/W) - 1 \tag{3}$$

At the compressor face, the flow coefficient is written, as in Eq. (53) of Ref. 1, preparatory to carrying out the Galerkin procedure

$$\phi_0 = \Phi(\xi) + WA \sin(\theta - r(\xi)) \tag{4}$$

The phase angle $r(\xi)$ is a function of time, as yet unknown. It will be found that this form is sufficiently general for present purposes; it is capable of bridging, in effect, between pure distortion (constant r) and pure rotating stall (r proportional to ξ).

At this point, the description of distortion as a single, fundamental harmonic wave may be questioned. The literature on distortion[6] discusses various wave forms, limited to sectors of various angular extent. Nevertheless, the data clearly show that the first harmonic of distortion is dominant; it would represent the chief result of inlet angle of attack, for example. In any event, the Galerkin procedure used in the present theory is able to take into account only the first harmonic of distortion because $\sin\theta$ and $\cos\theta$ are used as weighting functions in the averaging integrals.

The Galerkin procedure described in Ref. 1 may now be applied to Eq. (42) of that paper, modified to account for weak distortion by adding the terms

$$\epsilon h \cos\theta - \epsilon\Phi \sin\theta + \epsilon^2 \sin^2\theta$$

Although ϵ is assumed small, this modification may be shown to be correct to second order in circumferential disturbance due to distortion (that is, ϵ^2 or ϵA). The first of the foregoing terms is physically significant as a coupling between distortion ϵ and circumferential velocity disturbance h.

The Galerkin procedure gives the following equations from which system transients will be calculated:

$$P'(T) = \frac{1}{4(H/W)^2 B^2}(Q - Q_T) \tag{5}$$

$$Q'(T) = -P + \frac{3}{2}Q\left(1 - \frac{1}{2}A^2\right) - \frac{1}{2}Q^3 + \frac{\epsilon A}{2H/W}\cos r + \frac{\epsilon^2}{2W(H/W)} \tag{6}$$

$$A'(T) = K\left\{\frac{1}{2}A\left(1 - Q^2 - \frac{1}{4}A^2\right) - \frac{1}{3H/W}\left[\epsilon(Q+1) - \frac{\ell_d}{\ell_c}\frac{H/W}{W}\epsilon'(T)\right]\cos r\right\} \tag{7}$$

$$r'(T) = \frac{K}{3H/W}\left\{\frac{1}{2a} + \left[\epsilon(Q+1) - \frac{\ell_d}{\ell_c}\frac{H/W}{W}\epsilon'(T)\right]\frac{\sin r}{A}\right\} \tag{8}$$

These equations embody the cubic form of ψ_c discussed earlier. They also embody a redefined time variable T which, with other symbols, is defined in the Nomenclature.

Equation (5), like the identical Eq. (59) of Ref. 1, describes how the accumulation of mass in the plenum affects plenum pressure. Equation (6) deals with axial momentum and is identical to Eq. (60) in Ref. 1, except for the presence of the terms involving ϵ. The first of these, involving the product ϵA, results from the coupling already mentioned; it expresses a Magnus force in the axial direction experienced by a vortex filament of strength ϵ owing to distortion, when it is subject to a transverse velocity h which is proportional to A. The second term, proportional to ϵ^2, depends on the definition of average total pressure in Eq. (2).

Equation (7) also differs from its predecessor [Eq. (61) of Ref. 1, with $J = A^2$], in having terms containing ϵ. These equations allow for the possibility that distortion is itself time-dependent. When specific entrance flows are analyzed, it will be generally necessary to consider ϵ to be unsteady. In the present calculated examples, ϵ is constant, so that $\epsilon'(T) = 0$. Equation (7) deals with the growth of angular nonuniformity at the compressor face A, and shows that distortion indeed provides a seed for such rotating-stall-like disturbances.

Equation (8) is new, though it relates to Eq. (57) of Ref. 1. If there is no distortion, r must be linear in time T; then, in view of Eq. (4), any angular disturbance must be a wave of fixed and known constant angular velocity. That was the result of Ref. 1. Now, $r(T)$ is an unknown function which might be linear or even constant as in the case of distortion itself, depending on the behavior of A.

It has been mentioned that the foregoing equations are correct to order ϵ^2 and $A\epsilon$; that is, terms like $A^2\epsilon$, $A\epsilon^2$, and ϵ^3 have been neglected. The equations should then be especially useful when A is small; that is, when analyzing the destabilizing effects of distortion and its consequent effect on stall margin. Once a disturbance A has grown to unit order ($A = 2$ in pure rotating stall), the accuracy is only first order in ϵ; However, ϵ is found to have a rather small effect on fully developed transients anyway, so the loss of accuracy in those circumstances is not significant. It would, therefore, seem that the foregoing equations should be applicable for velocity distortion of 10%, and would, perhaps, have qualitative value for higher levels, such as 20%.

Finally, the system of transient equations is completed by adding the simple parabolic throttle equation

$$Q_T + 1 = GA\sqrt{P + PHO + 1} \tag{9}$$

The value of the throttle coefficient GA will fix the throttle line of interest in Fig. 3. For example, $GA = 1.265$ for the line labeled (1). GA may be a function of time T, to represent dynamic valve ramping.

For the analysis of a general transient, there are now five equations [Eqs. (5-9)] for five unknowns, which are all functions of time: P, Q, Q_T, A, and r. The next three sections will illustrate the application of this set of equations to problems of interest.

IV. Steady Results for Stall Margin

When the compressor is unstalled, perhaps at the throttle setting (S) in Fig. 3, the flow may be expected to be steady but nevertheless be influenced by inlet distortion. The given distortion pattern cannot be simply applied at the compressor face because the compressor will interact with and modify that pattern, just as in rotating stall.

Equations (5-9) can be used to show this steady interaction, simply by setting all time derivatives equal to zero and solving the resulting simultaneous equations for P, A, and r in terms of Q. [Equation (5) shows that $Q_T = Q$ in steady flow.] Since the governing equations are correct to second order in ϵ, and since A will be proportional to ϵ in this case, the algebraic solution may properly ignore terms of order A^3. The results are

$$P = \frac{3}{2}Q - \frac{1}{2}Q^3 - \epsilon^2\left[\frac{3a^2(Q+1)^2(2Q-1)}{1 + 9a^2(H/W)^2(Q^2-1)^2} - \frac{1}{2H}\right] \tag{10}$$

$$A = -\epsilon\frac{2a(Q+1)}{\sqrt{1 + 9a^2(H/W)^2(Q^2-1)^2}} \tag{11}$$

$$r = \operatorname{arccot}[2a(H/W)(Q^2-1)] \tag{12}$$

The first term in the brackets of Eq. (10) is typically much larger than the second, and it is clear that two parameters are important, $a(H/W)$ and ϵa.

The effects of these two parameters are shown in Fig. 4 for three combinations of values for diagram steepness H/W, reciprocal blade-passage lag a, and velocity distortion amplitude ϵ. The less important diagram width W was taken to be 0.5. Figure 4 focuses on the vicinity of maximum pressure rise. In each case, three curves are shown: A segment of the axisymmetric cubic characteristic labeled P, which is simply Eq. (10) with $\epsilon = 0$; steady performance with distortion labeled PD, which is Eq. (10) with the appropriate ϵ included; and the axial flow coefficient disturbance at the compressor face [see Eq. (4)] compared with the amplitude of distortion.

Instability is expected to be associated with the maximum of curve PD (as will be discussed in the next section), and the location of that maximum will, therefore, indicate steady stall margin. Two effects are evident in Fig. 4a: there is a loss of maximum performance due to distortion, and the maximum occurs at higher flow rate Q. In Fig. 4b, the parameters were changed so that ϵa was increased leaving $a(H/W)$ the same. The result is a further decrease of maximum performance at a somewhat larger Q. In Fig. 4c, ϵa was kept the same as in Fig. 4b, but the effective steepness $a(H/W)$ was greatly reduced. Now although the loss of performance is nearly unchanged, the maximum has shifted to smaller Q. In effect, the hump evident in the first two cases has disappeared.

Roughly, it may be said that the value of ϵa governs the loss of maximum performance due to distortion, while the value of $a(H/W)$ governs the margin or minimum Q for stable flow. Apparently, the location of the maximum is either substantially to the right or left on the diagram; the critical value of $a(H/W)$ is about 1, with higher values being associated with reduced margin.

In view of the importance of $a(H/W)$, its physical significance should be examined. As discussed in Refs. 1 and 5, if the blade-passage lag is inertial, then [see Eq. (25) of Ref. 1] a is inversely proportional to the blade-passage flow length ℓ_B and the number of stages. That is

$$a \simeq (\cos\gamma)/(N\ell_B) \tag{13}$$

H/W is proportional to stage loading and also to number of stages. Thus, the product $a(H/W)$ depends chiefly on blade passage length ℓ_B. Perhaps the suggestion is warranted that large values of blade passage length (relative to rotor radius) would improve stall margin. Since the distortion level is also coupled with a in the parameter ϵa, it might also be supposed that the loss of maximum pressure rise due to distortion would be reduced by increasing the total flow-passage length of the compressor, $N\ell_B$.

Independently, Hynes and Greitzer[10] have provided a stability analysis of the effect of inlet distortion with an underlying philosophy similar to the present one. Their theory does not embody the Galerkin method, and they are able to assess the effects of all harmonics, not just the fundamental as in this study. However, their analysis is linear in ϵ, unlike the present one, which is second order in ϵ. In the present study, it has been shown that the steady effect of distortion emerges as an aspect of the general transient behavior. In the next section, unsteady transients leading to surge and rotating stall are examined. Such transients may originate in steady flows which are influenced by distortion.

V. Dynamic Results for Stall Throttle Closure

Equations (5–9) will now be used to determine the result of closing the throttle, beginning at an unstalled condition (such as Ⓢ in Fig. 3) and ending at a condition (one of the lines Ⓕ) in which stall might be expected. Figure 5 shows the ramp process for throttle coefficient GA; closure is at a given constant rate GS, until the final value GA_F is reached, after which the throttle setting stays constant. As a typical problem, GA_F is taken slightly to the stalled side of the maximum pressure rise, where $Q_F = 0.9$, so that the stall will be definite. Using Eq. (9) and Fig. 1, Table 1 collects certain numerical values of GA for future reference, including those applicable for $Q_F = 0.9$.

As a basis for comparisons to come, a standard or base case is specified as a set of typical values of system parameters. Table 2 defines the base case. A quite small distortion level of 1% has been chosen. This will be large enough to act as a trigger, but is surely small enough to insure accuracy of the governing equations. B and PHO are left undefined in Table 2. The rate of throttle closure is 0.01 in this section, unless otherwise specified. Such a ramp rate is slow enough not to affect the development of instabilities.

Figures 6–9 show certain typical results obtained by integrating Eqs. (5–9) for the base case. (Calculations were done by first-order forward time marching, using an IBM PC.) Each transient was started from the appropriate steady solution [Eqs. (10–12)], lying on the specified initial throttle line. When $B = 1.8$ and $PHO = 0.5$, throttle closure from Ⓢ leads to a "deep-surge" (DS) limit cycle, following the arrows in a counterclockwise direction. The spacing between dots indicates speed; the horizontal segments are relatively very

Table 1 Throttle coefficients

PHO	0.5	1.0	1.5	2.0
GA_3	1.500	1.265	1.123	1.026
GA_2	1.410	1.161	1.010	0.906
GA_1	1.265	1.155	1.069	1.013
GA_F for				
$Q_F = 0.90$	1.202	1.097	1.016	0.950
$Q_F = 0.80$	1.138	1.039	0.962	0.900

Table 2 Base case for cycle calculations

Parameter	Value	Interpretation
a	0.6	Reciprocal time lag of blade-passage pressure rise when responding to axial flow change
B	Variable	Reflects plenum volume, $B = (U/2a_s)\sqrt{V_p/A_c\ell_c}$
GA	variable	throttle coefficient related to K_T (see Table 1)
GS	−0.01	Rate of throttle closing (Fig. 5)
GS	−0.006	Rate of throttle closing and opening (Fig. 16)
H/W	0.75	Height-to-width ratio of axisymmetric characteristic, proportional to number of stages
ℓ_c	8.0	Dimensionless length of flow ℓ_c path through entrance duct, compressor, and exit duct
m	1.75	Parameter depending on aerodynamics of entrance and exit ducts
PHO	Variable	Shut-off head rise coefficient in ratio to H, inversely proportional to stage loading
W	0.5	Width of axisymmetric characteristic
ϵ	0.01	Amplitude of inlet distortion of axial flow coefficient

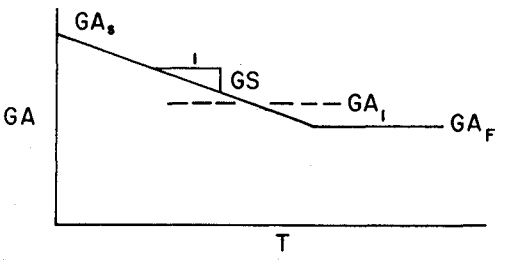

Fig. 5 Throttle ramp to stall. Starting at setting GA_s, throttle is closed at rate GS, then held at setting GA_F in a stalled condition. Process corresponds to arrow on Fig. 3.

quick. In the same diagram, the level of circumferential nonuniformity is also shown, as $J=A^2$, for convenience. The excursion of J to a level about half that which would typify pure rotating stall occurs during the rapid fall of Q in each cycle. It would not occur at all if there were no distortion; however even though ϵ is only 0.01, its presence triggers a large excursion of J. The same effect was found in Ref. 2 when small initial values of J itself were postulated.

The same oscillation is shown as the time trace which a single, fixed axial-velocity probe would theoretically measure at the compressor face; that is, ϕ_0/W as given in Eq. 4. The predicted period is about 35 time units which, for the base case, is about 60 wheel revolutions. The small wiggle in the trace at about $T=80$ reflects the excursion of J shown on the cycle diagram.

Figure 7 shows the effect of reducing B to 1. As was learned from Ref. 4 and found in Ref. 2, the smaller B conduces to rotating stall. When the throttle passes through the maximum pressure point, a small loop appears (corresponding to the slight wobble of the time trace at about $T=50$), and then the transient falls directly to point O_F', which is the middle of the three operating points labeled (F) in Fig. 3. It lies on the characteristic for pure rotating stall (RS) and, therefore, constitutes a case of "stagnation stall." J (that is, A^2) rises very rapidly following the onset of instability and then also ends up at a fixed value, namely that given for RS in the upper curve of Fig. 2. Although the final state is stationary as regards P and Q, the time trace shows a vigorous rotating stall in progress, described as a harmonic wave in the Galerkin formulation. Its period is about 4 wheel revolutions.

For finite distortion, the final state is not really stationary because the rotating stall pattern and the fixed distortion pattern are in a constantly shifting phase relationship. This is illustrated by Fig. 8, which repeats the previous case, but with 20% rather than 1% distortion level. As the previous section on steady stall margin would suggest, the unstalled track is at a lower pressure level, and because $a(H/W)$ is 0.45, the maximum is expected to be at some $Q<1$. The throttle transient again produces rotating stall, but the final states of both P and J are not fixed; instead, they oscillate in counterclockwise loops about the pure RS points. The loop amplitudes scale with ϵ.

With distortion returned to its base value of $\epsilon=0.01$, PHO is next increased to 2.0, and the transient takes a different form having the nature of a surge loop, but not extending to reverse flow. This sort of cycle, shown in Fig. 9, is commonly called "classic surge" (CS), as described in Ref. 4. There are episodes of fully developed rotating stall in this cycle; J reaches the level (4) of pure RS in its cycle. The time trace makes clear how this oscillation proceeds as a kind of hybrid of DS and RS. The period is about 25 revolutions, intermediate between the deep surge and rotating stall cases seen earlier.

If B is returned to 1.8, where deep surge was found when PHO was 0.5, and PHO now is kept at 2.0, the stall transient shown in Fig. 10 is found. The instability begins with a weak rotating stall followed by a vigorous rotating stall, which in turn develops into a deep surge of rather short period (about 35 revolutions).

Stability of Rotating Stall

The foregoing examples show that, depending on the values of B and PHO, a wide variety of transient motions can result from throttle closure. Further calculations show that this behavior can be well described on the map of $B(H/W)$ vs PHO, displayed in Fig. 11. The reason for grouping B with H/W is made clear later. For small PHO, a base-case transient will become deep surge if $B(H/W)$ is large enough. Figure 6 refers to such a case with $B(H/W)=1.35$. If that quantity is smaller than the critical value indicated as a solid line in Fig. 11, then rotating stall results. For PHO of 2.0, deep surge again results if $B(H/W)$ is above the dot-dashed critical line

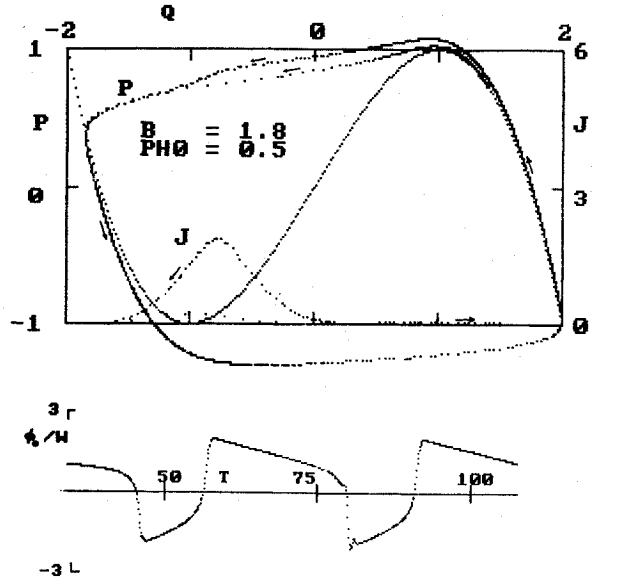

Fig. 6 Limit cycle ($P-Q$) for "base case" (see Table 2) with $B=1.8$, $PHO=0.5$. Result is "deep surge" (DS). J varies during cycle as shown. Axial flow coefficient seen by a fixed probe vs dimensionless time T is shown below.

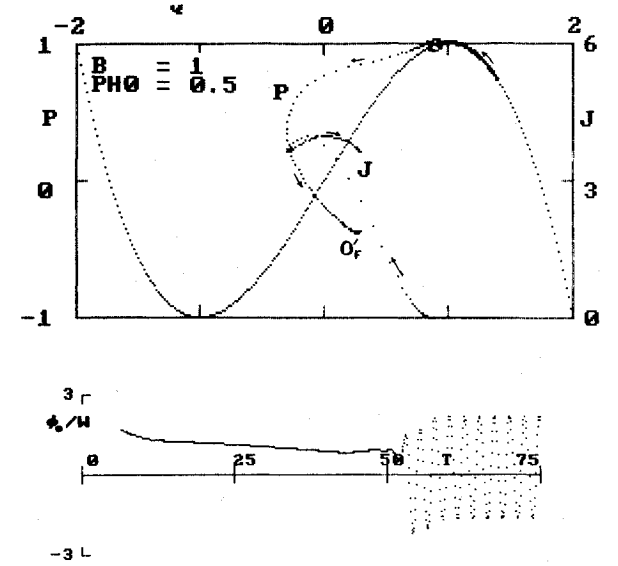

Fig. 7 Stagnation stall in base case with $B=1$ and $PHO=0.5$. Final state is at point O_F' of Fig. 3. J reaches equilibrium (Galerkin) result for that Q. Probe would see pure rotating stall (RS) after $T=60$.

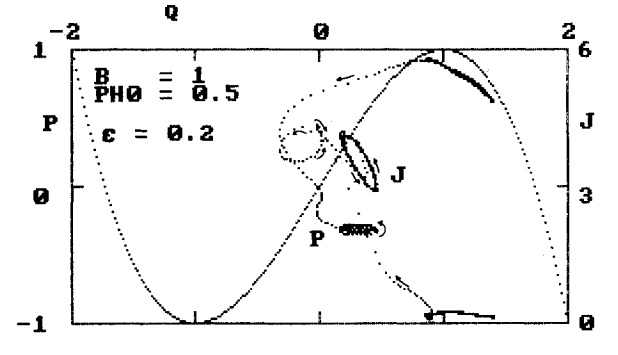

Fig. 8 Stagnation stall (RS) for the same case as Fig. 7, except that distortion level is much higher (0.20 instead of 0.01). Both P and J perform loops of amplitude ϵ about point O_F'.

(Fig. 11), and rotating stall results below the dashed line; however, between those two critical lines, classic surge is found (Fig. 9). The transition between the small and large *PHO* regimes is very abrupt, as Fig. 11 shows. It is concluded that large *PHO* or, in effect, low stage loading favors classic surge, while high stage loading favors rotating stall.

Searching for a reason for this sudden change with *PHO*, one notices in Fig. 3 that there is always some *PHO* for which the final throttle line (passing through $Q_F = 0.9$ in the base case) cuts the rotating-stall performance curve at its relative minimum point O_2', which defines a possible operating point in pure rotating stall. In the base case, that special value of *PHO* is 1.45. For any other final throttle setting, Fig. 12 gives the corresponding critical *PHO*.

In Fig. 11, the central circled sketch shows the critical situation just described. For $PHO < 1.45$, the sketch shows that the operating-point intersection is at a negative slope, while for $PHO > 1.45$, the slope is positive. Negative characteristic slope is associated with stability and positive with instability. In this case, the stability consideration concerns rotating stall because the characteristic in question is that for pure rotating stall. Therefore it may perhaps be concluded that rotating stall is relatively suppressed at large *PHO* because it itself becomes unstable as a mode of operation. It should be noted that rotating stall does not altogether disappear when $PHO > 1.45$, except possibly in the infinite limit.

Figure 13 shows how the map of Fig. 11 changes when the final throttle setting differs from the base case. If the throttle is left more open (Q_F nearly 1), then transitions occur at higher $B(H/W)$ for both small and large *PHO*; however, the critical *PHO* is lower, as Fig. 12 predicts. If the final throttle is more closed ($Q_F = 0.8$), critical *PHO* is higher, 2.09, which is just off the scale of Fig. 13, and the transitions are at lower $B(H/W)$. Apparently, as Q_F decreases, the surge instability

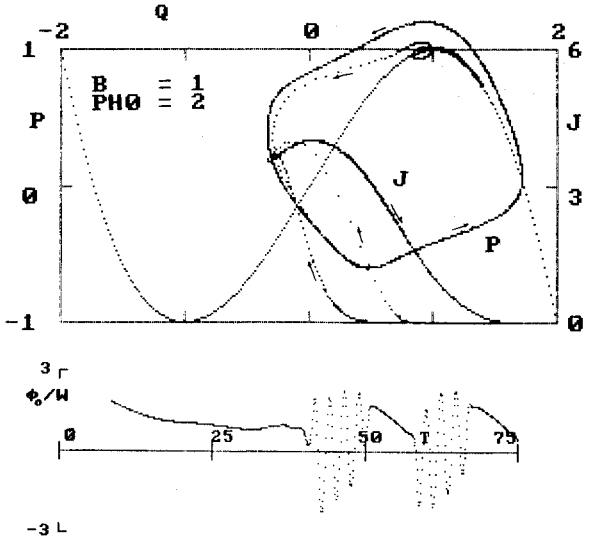

Fig. 9 Classic surge (CS) of base case occurring at $B = 1.0$, $PHO = 2.0$ (compare Fig. 6 for same B).

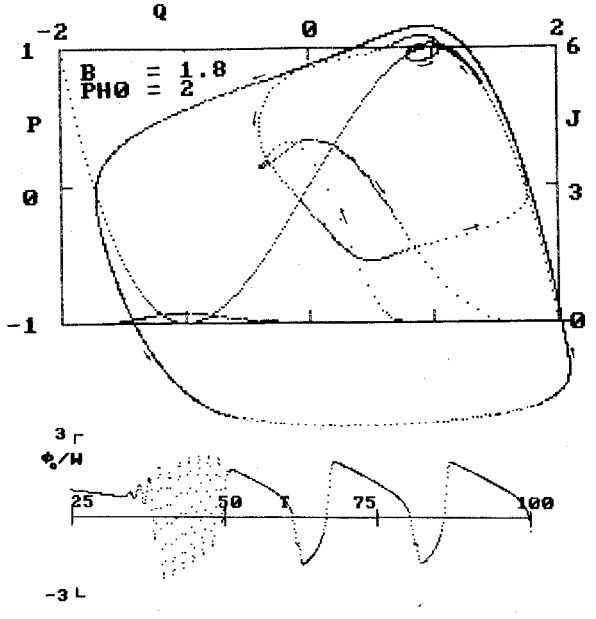

Fig. 10 Base case ($\epsilon = 0.01$) for $B = 1.8$, $PHO = 2.0$. A "progressive" transient leads to limited surge transient, and finally deep surge.

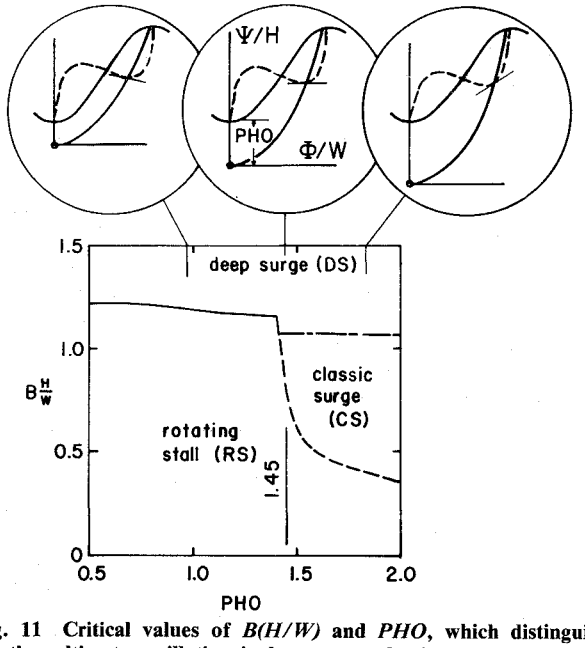

Fig. 11 Critical values of $B(H/W)$ and *PHO*, which distinguish whether ultimate oscillation is deep surge, classic surge, or rotating stall, for base case defined in Table 2.

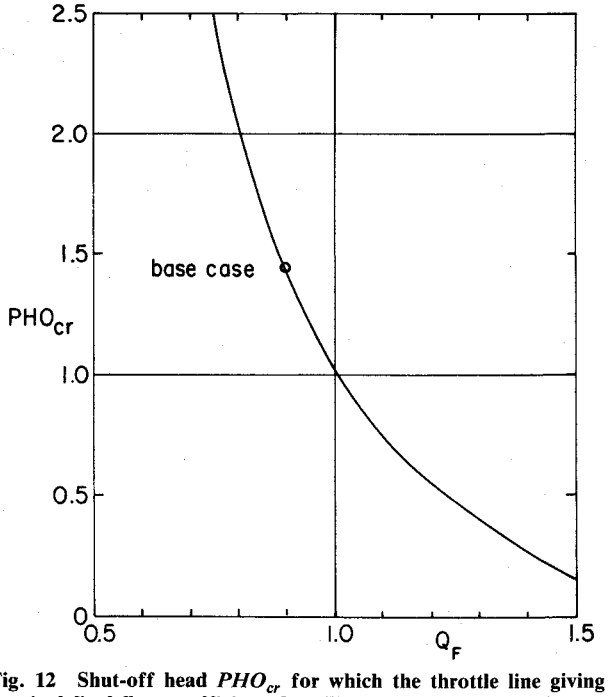

Fig. 12 Shut-off head PHO_{cr} for which the throttle line giving a nominal final flow coefficient Q_F will pass through the minimum of the RS characteristic (point O_2' of Fig. 3).

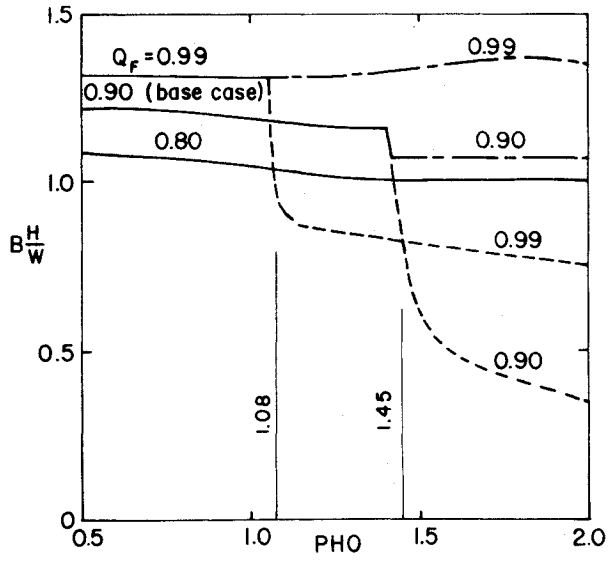

Fig. 13 Effect of final throttle setting on surge boundaries, comparing the base case $Q_F = 0.9$ with the more open $Q_F = 0.99$ and the more closed $Q_F = 0.8$ cases.

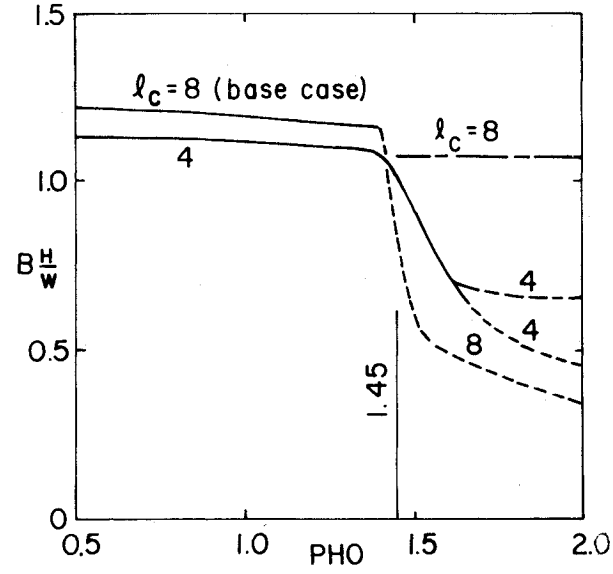

Fig. 14 Effect on the surge boundaries of a reduction of ℓ_c, the compression flow length.

indicated by greater positive slope of ψ_c become relatively more important than the increase of rotating-stall "stability" implied by negative slope of its own characteristic.

Effects of System Changes

Final throttle setting is just one of the changes which may be made in the base case to explore how the transition boundaries between deep and classic surge and rotating stall depend on system parameters.

Next, the effect of the flow lengh ℓ_c is considered. Figure 14 shows the effect of changing ℓ_c from 8.0 (the base case) to 4.0. The chief effect is to suppress classic surge in favor of deep surge at large *PHO*. There is also a tendency to suppress rotating stall at small *PHO*. The tendency of small ℓ_c to favor surge against rotating stall was noted in Ref. 2, and that result was explained by noting that smaller ℓ_c tends to reduce the rate of growth to rotating stall relative to that of a surge disturbance. Here, ℓ_c appears only in the parameter K which indeed governs the growth of A, according to Eq. (7). A suppression

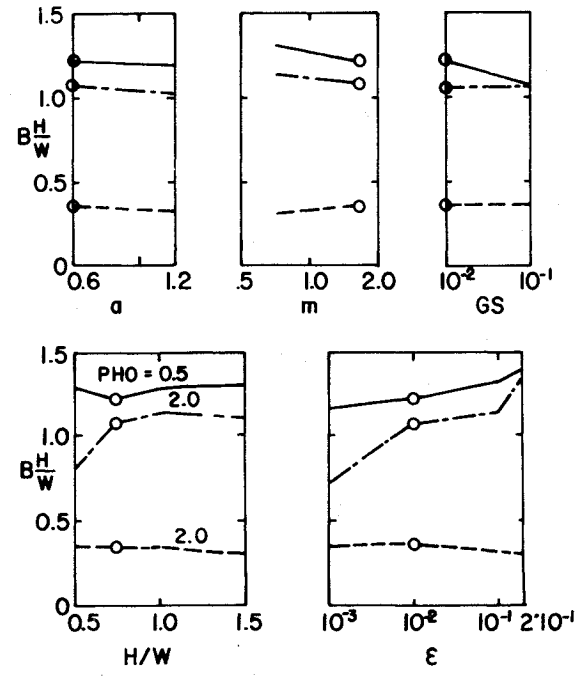

Fig. 15 Effects of parameters on main features of surge boundaries. In each case, upper line refers to the DS-RS boundary at $PHO = 0.5$, the middle line the DS-CS boundary at $PHO = 2.0$ and the lower line the CS-RS boundary at $PHO = 2.0$.

of A will not only suppress final rotating stall, but also those RS-like episodes which distinguish classic from deep surge in present terminology.

Figure 15 shows the effects of modifying the other parameters which define the base case of Table 2. Only the changes of the DS-RS transition boundary of Fig. 11 at $PHO = 0.5$ and the changes of the DS-CS and CS-RS transition boundaries at $PHO = 2.0$ are shown as functions of parameter changes. For each boundary, the base case is denoted by a circle. The effect of changing H/W over a factor of three is quite small, unless the diagram is very shallow. Thus, it seems appropriate to think of the product $B(H/W)$ rather than B alone in its influence on the choice between surge and rotating stall.

Not surprisingly, a large distortion level clearly favors rotating stall over surge and also favors classic over deep surge. Significant distortion gives rotating stall a head start, so to speak, in its competition with surge. The effect is only significant beyond $\epsilon = 10\%$, however. For $\epsilon < 1\%$, classic surge is apparently suppressed. It is found that the RS-like episodes, which accompany even deep surge, are very strong when $\epsilon = 10\%$, are present but not strong when $\epsilon = 1\%$ (as in Fig. 6), and vanish entirely when $\epsilon = 0.1\%$. In Ref. 2, it was found that the growth of A depends on A itself. In the present study, the presence of A depends on distortion, and its growth depends on distortion level ϵ and A together. Therefore, while distortion as small as 0.1% can trigger stagnation stall, it is not strong enough to permit RS to participate in a surge oscillation of either the classic or deep type.

Figure 15 shows that neither a nor m have an important direct effect on the transitions of interest. References 5 and 9 indicate that a small value of m, which would be associated with a strongly convergent entrance duct or a short diffuser in combination with a "tall" axisymmetric characteristic, would tend to prevent rotating stall. That result is not available from an analysis of pure RS in the present Galerkin study. Future more exact combined-cycle studies may well show that m is, in fact, a very important parameter for stall recovery.

Finally, the throttle ramping rate GS (Fig. 5) is increased by a factor of 10, still leaving the final throttle setting at $Q_F = 0.9$. It might be expected that a more sudden throttle movement

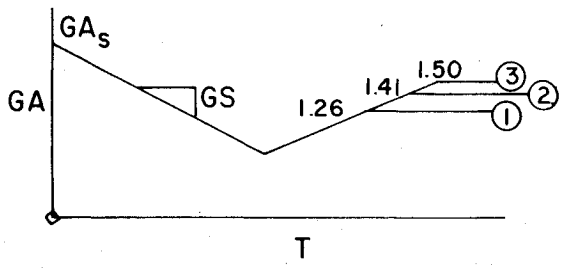

Fig. 16 Schematic of throttle ramp to stall and then recovery. Throttle closed at Rate *GS* to stalled condition, then opened at the same rate to some final setting (which might be lines ①, ②, or ③ of Fig. 3), and then held constant. Corresponding values of *GA* are shown.

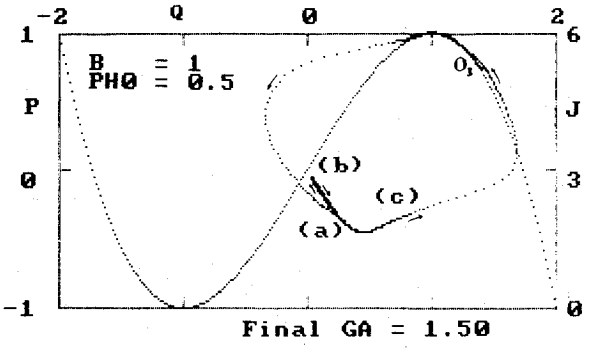

Fig. 17 Recovery from rotating stall if final throttle setting is line ③ of Fig. 3. (a) in RS; throttle continues to close to point (b); throttle opens until line passes through point O_3', but performance recovers starting at about point (c), finally reaching point O_3.

would favor surge because the initial effect, at least, would be surge-like. Indeed, that is what is found, but only for subcritical values of *PHO*; for larger values of *PHO*, ramping rate seems not to be important.

VI. Dynamic Results for Stall Recovery

A stall transient resulting from closing the throttle may culminate in surge of the deep or classic types, or rotating stall. Then, the question arises of how recovery occurs when the throttle is opened again. In general, hysteresis is observed in such a process, and the present theory will now be used to demonstrate and as, to some extent, explain that phenomenon.

The base-case system (Table 2) will be assumed, and the throttle will first be slowly closed at a rate $GS=-0.006$, beginning at a suitable unstalled condition, until a thoroughly stalled condition is achieved at $GA=0.86$. Then, as Fig. 16 describes, the throttle will be slowly opened again at the same rate, but then it will be stopped and held at some throttle setting of interest. The question will be whether the system then recovers to a unstalled condition. Three final throttle settings of interest are indicated in Fig. 16 and defined in Fig. 3.

Recovery from Surge

It has been shown in the previous section that if $B(H/W)$ and *PHO* are chosen so that the closure phase of throttle movement results in surge, it develops promptly when the throttle passes through the characteristic maximum at $Q=1$. In such a case, if the throttle continues to close, Fig. 13 shows that surge would be expected to continue because the given $B(H/W)$ would find itself progressively farther above the surge transition boundary, as the latter moves downward with throttle coefficient. When the throttle reverses and opens to the original point of instability ($Q=1$, at throttle line ①), one might expect recovery from surge to occur. In effect, there would be no hysteresis. The reason recovery would be expected at ① is that during each surge cycle, the system spends a very long time slowly climbing the unstalled characteristic,

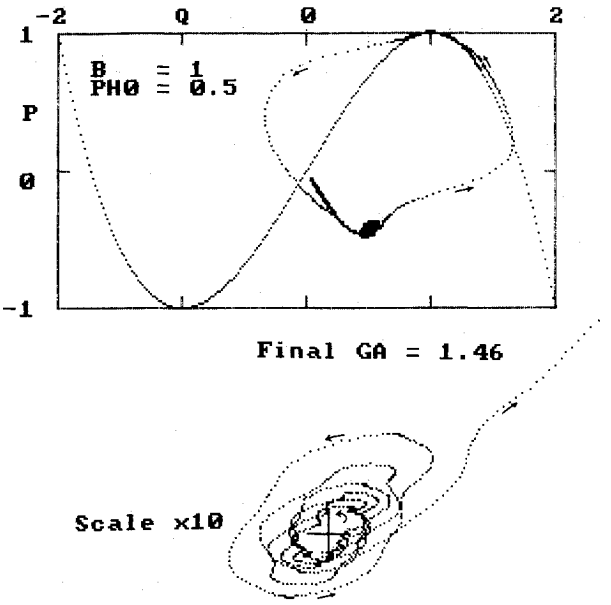

Fig. 18 Recovery for same case as Fig. 17, except throttle closed to setting midway between ② and ③.

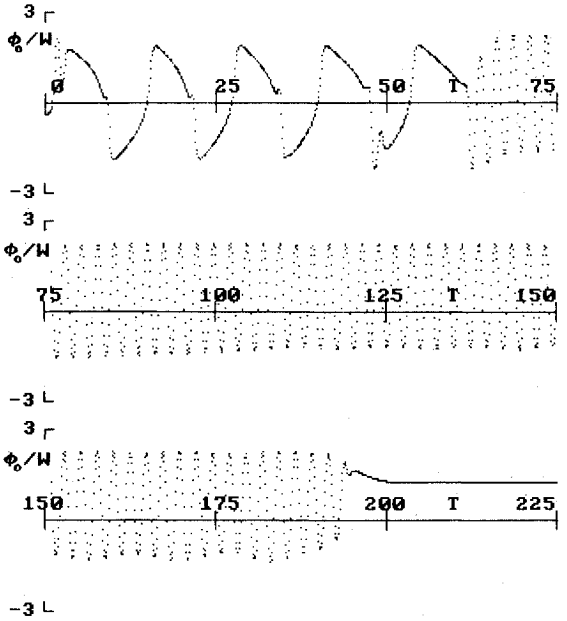

Fig. 19 Same problem as Fig. 18, except that the closure is much faster ($GS=-0.100$ instead of -0.006). Opening process is the same. Surge first occurs, but midway in the opening process rotating stall takes over.

and after the throttle reaches a stable position at ①, the oscillation should simply stop at that point, $Q=1$, the next time it arrives there.

Calculations indicate that the foregoing type of recovery is the usual one. However, in one case, recovery from surge did not occur; rather, the oscillation dropped into rotating stall when the throttle approached ①. The throttle would have to be opened still further in order to cause RS to recover, and hysteresis would therefore be implied. This event is not fully understood, but it certainly concerns the relation of the phase of surge to throttle position and perhaps depends on throttle opeing rate. Rotating stall would not have resulted from throttle closure in that instance, and it is not obvious why it should happen on opening. It must be concluded that surge recovery is sensitive to phase and may occasionally involve hysteresis. Further study should be given to this question, and the process of recovery from classic surge should also be considered.

Recovery from Rotating Stall

B and *PHO* may be chosen so that rotating stall results immediately from closing the throttle past position (1) of Fig. 3. A base-case example is shown in Fig. 17. The transient goes into rotating stall at point (a), and as the throttle continues to close in accordance with Fig. 16, a segment of the in-rotating-stall characteristic (dashed line of Fig. 3) is traced out until point (b) is reached. Then, the throttle begins to open again, and the pressure rise continues to follow the RS characteristic for a while. In this particular case, the throttle is stopped at position (3), or $GA = 1.50$, which is the most-open throttle line that still touches the RS characteristic. Figure 17 shows how the transient recovers from point (c) after the throttle reaches its final position. The oscillation terminates at point O_3', which is the unstalled operating point for line (3). In this case, lines (1) and (3) form a hysteresis loop. The width of the hysteresis obviously depends on *PHO*; the loop would be narrow for large *PHO*.

The question arises whether the throttle must open all the way to position (3) in order for rotating stall to recover. The discussion of "stability of rotating stall" contained in the previous section suggests that perhaps recovery might occur if the throttle is stopped anywhere between (2) and (3) in Fig. 3, on the grounds that the RS characteristic has an "unstable" slope in that interval. To test this idea, the case of Fig. 17 was repeated with the throttle opening terminated at $GA = 1.46$ (see Table 1), which is about half-way between (2) and (3). The result is shown in Fig. 18. The stall process of Fig. 17 is repeated, except that the transient stays at the appropriate RS operating point between O_2' and O_3' for about 90 time units or about 150 wheel revolutions, but then ultimately recovers. During those 90 time units, a small loop slowly grows, as shown on the expanded scale, until it finally becomes unstable and recovery follows.

Thus, it is concluded that the concept of rotating-stall stability has some validity, and the hysteresis associated with rotating stall depends to some degree on the particular profile of throttle movement that is imposed.

An interesting variant of the last problem is shown in Fig. 19. The case is exactly the same, except that the throttle is closed much faster with $GS = -0.1$ rather than -0.006; then, the throttle is slowly opened as before. The result, shown as a theoretical probe trace, is that deep surge is caused by the suddenness of the throttle closing; it persists for about 50 time units after the closing is finished, and then it transforms to rotating stall. The throttle opening process is complete when T is about 115; after that, recovery occurs as in Fig. 17. Probably, when the throttle is most closed, surge should be expected, even though $B = 1$. Then, when the throttle is opened, and the transition line of Fig. 13 moves up, RS becomes favored again. Contrasting Figs. 18 and 19, it would seem that in the latter case, fast throttle closure allows surge to survive to the small throttle openings where it is favored, whereas, when the throttle is slowly closed, rotating stall becomes established first and persists even down to throttle settings for which surge would otherwise be expected. Thus, a kind of dynamic hysteresis is indicated.

VII. Conclusions

A previously derived system of differential equations governing stall transients of axial compression systems was extended to include inlet total-head distortion. The equations were first applied to the steady effect of inlet distortion on unstalled performance. Loss of maximum pressure depends mainly on the product of distortion level and a reciprocal flow path length through the compressor. Stall margin (in terms of flow coefficient) is reduced in proportion to chiefly the steepness ratio of the axisymmetric characteristic and, again, inversely to the compressor flow-path length. It is interesting that dynamic aerodynamic lag in the compressor affects steady performance when there is inlet distortion.

The equations were then used to assess the influences of various parameters on throttle-induced stall and recovery from stall. When stall is caused by throttle closure, one finds that deep surge (DS) is favored not only by large values of the familiar *B* parameter, but also by diagram steepness (number of stages and blade turning). When stage loading is large, reduction of *B* or steepness leads to a transition from DS directly to rotating stall (RS); but when stage loading is low, there are two transitions: an upper one from DS to classic surge (CS) and a lower one from CS to RS. The critical stage loading (*PHO*, in effect) occurs when the throttle line passes through the minimum of the in-RS characteristic, as distinct from the axisymmetric one. When the throttle is more open than that, RS is in a sense unstable.

A more fully closed throttle favors surge; rapid closure (ramp rate) also favors surge. High levels of distortion, on the other hand, favor RS. Even less than 1% distortion can trigger RS, and above a few percent, RS always appears as a cyclic feature of surge.

Analysis of stall recovery shows recovery from surge when the throttle reaches the maximum of the axisymmetric characteristic. Thus, there is generally no hysteresis in that case; although in one instance, which merits further study, DS dropped into RS just before recovery. Recovery from RS occurs when the throttle is between the minimum of the RS characteristic and the point of osculation with that characteristic, consistent with an idea of RS stability. Hysteresis will characterize RS inception and recovery.

It seems possible that most essential features of system transients can be predicted with knowledge of pure RS and pure DS performance, together with certain principles concerning axisymmetric and RS characteristics and their stability implications.

Acknowledgments

This research has been supported by NASA through the Lewis Research Center by Grant NAG-3-349. Contributions by F. E. McCaughan and J. S. Mathur, graduate students at Cornell, are acknowledged.

References

[1]Moore, F. K. and Greitzer, E. M., "A Theory of Post-Stall Transients in Axial Compression Systems. Part I—Development of Equations," *Journal of Engineering for Gas Turbines and Power*, Vol. 108, Jan. 1986, pp. 68–76.

[2]Greitzer, E. M. and Moore, F. K., "A Theory of Post-Stall Transients in Axial Compression Systems. Part II—Applications," *Journal of Engineering for Gas Turbines and Power*, Vol. 108, April 1986, pp. 231–239.

[3]Moore, F. K. and Greitzer, E. M., "A Theory of Post-Stall Transients in Multistage Axial Compression Systems," NASA CR 3878, March 1985.

[4]Greitzer, E. M., "Surge and Rotating Stall in Axial Flow Compressors, Parts I, II," *Journal of Engineering for Power*, Vol. 98, April 1976, pp. 190–217.

[5]Moore, F. K., "A Theory of Rotating Stall of Multistage Axial Compressors, Parts I, II, III," *Journal of Engineering for Power*, Vol. 106, April 1984, pp. 313–336.

[6]Bowditch, D. N. and Coltrin, R. E., "A Survey of Inlet Engine Distortion Compatibility," NASA TM 83421, 1983.

[7]Koff, S. G. and Greitzer, E. M., "Stalled Flow Performance for Axial Compressors—I: Axisymmetric Characteristics," ASME Paper 84-GT-93, 1984.

[8]Day, I. J., Greitzer, E. M., and Cumpsty, N. A., "Prediction of Compressor Performance in Rotating Stall," *Journal of Engineering for Power* Vol. 100, Jan. 1978, pp. 1–14.

[9]Joseph, S. T., "Effect of Compressor Parameters on Rotating Stall," M. S. Thesis, Cornell University, Ithaca, NY, Jan. 1985.

[10]Hynes, T. P. and Greitzer, E. M., "A Method for Assessing Effects of Circumferential Flow Distortion on Compressor Stability," presented at ASME Winter Annual Meeting, Dec. 1984, to be published in *Journal of Engineering for Gas Turbines and Power*.